CHEMIJA. 2021. Vol. 32. No. 2. P. 63–72

Investigation of upconversion phenomenon in $Y_{1-x}Ln^{3+}_{x}(BTC)(DMF)_2(H_2O)$ and $Y_{0.8-x}Yb_{0.2}Ln^{3+}_{x}(BTC)(DMF)_2(H_2O)$ metal organic frameworks

Andrius Laurikėnas[1, 2*],

Aivaras Kareiva[1]

[1] *Institute of Chemistry, Vilnius University, 24 Naugarduko Street, 03225 Vilnius, Lithuania*

[2] *Department of Organic Chemistry, Center for Physical Sciences and Technology, Saulėtekio Avenue, 10257 Vilnius, Lithuania*

In this study, $Y_{1-x}Ln^{3+}_{x}(BTC)(DMF)_2(H_2O)$ and $Y_{0.8-x}Yb_{0.2}Ln^{3+}_{x}(BTC)(DMF)_2(H_2O)$ metal organic frameworks (MOFs), which structure included lanthanide ions, Ln^{3+} (Er^{3+}, Ho^{3+}, Tm^{3+}, Yb^{3+}, Nd^{3}), suitable for monitoring the upconversion phenomenon, have been synthesised. For this purpose the precursor of the organic moiety, benzene-1,3,5-tricarboxylic acid (BTC), as one of the simplest and very frequently cited carboxylic acid analogues in MOF syntheses, has been selected. By characterising upconversion properties of new MOFs it was determined that only Er^{3+} can be used as an activator for one centre luminescence upconversion by a ground state absorption/excited-state absorption (GSA/ESA) mechanism, while with Yb^{3+}, Ho^{3+}, Tm^{3+} and Nd^{3+} ions the upconversion was not observed. It was also established that BTC cannot initiate triplet–triplet annihilation upconversion (TTA-UC) as this mechanism sensitizer. Yb^{3+}–Er^{3+} and Yb^{3+}–Ho^{3+} ion pairs as a sensitizer-activator were suitable for two-centre luminescence upconversion by a GSA/excited-state upconversion (GSA/ESU) mechanism. A pair of Yb^{3+}–Tm^{3+}, contrary as shown in the literature review, does not exhibit upconversion properties in the synthesised MOFs.

Keywords: metal organic frameworks, lanthanide ions, BTC, luminescence, upconversion

INTRODUCTION

One of the pioneers of a successful study of the phenomenon of upconversion was Auzel, who in 1966 first raised the idea that energy transfer between rare earth RE ions can occur between two cations, both of which are in the excited state when energy transfer takes place in the initial stage [1]. Er^{3+}–Yb^{3+} and, shortly afterwards in another publication, Tm^{3+}–Yb^{3+} trivalent ion pairs were the first among which Auzel experimentally observed the conversion in 1966. These experiments were published separately by Ovsyankin with Feofilov in the same year, only they added a pair of Ho^{3+}–Yb^{3+} ions to these two pairs [2]. In addition to Er^{3+}, Tm^{3+} and Ho^{3+} ions, which are still the most commonly used in conversion studies, Pr^{3+} and Nd^{3+} are used, much less some remaining Ln^{3+} (Tb^{3+}, Eu^{3+}, Sm^{3+}, Dy^{3+}), as well as several transition metals or actinides [1, 3].

Since 1997, a new class of the high-ordered and high-porosity materials, metal-organic frameworks (MOFs), began to be produced and investigated actively [4]. Such structures caused a great interest for researchers in regard to their unique structural, physical and chemical characteristics, providing an opportunity for their application in various areas of

* Corresponding author. Email: andrius.laurikenas@chgf.vu.lt

technology and science [5–8]. MOFs are very versatile – a modular structure, consisting of inorganic nodes connected between organic linkers, allows carrying out purposeful designing of material with the specific functionality, predictable morphology and chemical properties. Synthesis capability of hybrid materials with predictable properties on the basis of MOF distinguishes them from classical solid-state materials, in particular from traditional porous materials, such as mesoporous silicon dioxide and activated carbon.

In the present day, the most attention of scientific investigations is put on the synthesis and structural characterisation of new MOFs, analysis of their physical and chemical properties and post-synthetic modification. MOFs can be used in gas storage and separation [9–12], serve as catalysts [13–17] and luminescent materials [18–21]. However, today only about 14 MOFs are commercially available [22], mostly produced by Baden Aniline and Soda Factory (BASF), Germany. Because of their limited availability, MOFs could not force out usual adsorbents, catalysts and other materials yet.

In the present study, metal organic frameworks $Y_{1-x}Ln^{3+}_x(BTC)(DMF)_2(H_2O)$ and $Y_{0.8-x}Yb_{0.2}Ln^{3+}_x(BTC)(DMF)_2(H_2O)$, which structure included lanthanide ions Ln^{3+} (Er^{3+}, Ho^{3+}, Tm^{3+}, Yb^{3+}, Nd^{3}), possibly suitable for monitoring the upconversion phenomenon were synthesised and investigated.

EXPERIMENTAL

All reagents used in the synthesis were used without further purification. Benzene-1,3,5-tricarboxylic acid (BTC) was purchased from Glentham Life Sciences. Methanol (MeOH), N,N-dimethylformamide (DMF) and sodium acetate trihydrate ($NaOAc{\cdot}3H_2O$) were purchased from Chempur. Yttrium (III) nitrate hexahydrate ($Y(NO_3)_3{\cdot}6H_2O$) (99.9% pure) was purchased from Alfa Aesar. Other salts of lanthanides, ytterbium (III) nitrate pentahydrate ($Yb(NO_3)_3{\cdot}5H_2O$), thulium (III) nitrate pentahydrate ($Tm(NO_3)_3{\cdot}5H_2O$), erbium (III) nitrate pentahydrate ($Er(NO_3)_3{\cdot}5H_2O$), holmium (III) nitrate pentahydrate ($Ho(NO_3)_3{\cdot}5H_2O$) and neodymium (III) nitrate hexahydrate ($Nd(NO_3)_3{\cdot}6H_2O$), all 99.9% pure, were purchased from Sigma-Aldrich®.

X-ray diffraction (XRD) measurements of all synthesised compounds were recorded in the 2θ range between 5–70° with a Rigaku Miniflex II diffractometer (Cu Kα radiation with a graphite monochromator). Thermogravimetric analysis (TGA) of the samples was performed with a Perkin Elmer STA6000 thermal analyzer in air up to 900°C at 5–10°C min^{-1}. The morphology of the samples was investigated with scanning electron microscopes – Hitachi TM3000 and Hitachi SU-70. For the upconversion data analysis, emission spectra were recorded using an Edinburgh Instruments FLS 980 spectrofluorimeter. Measurements were made in a wavelength range of 350 to 800 nm by recording the measurement step every 0.5 nm. The compounds were excited by laser radiation at a wavelength of 980 nm, and the maximum laser current intensity used was up to I = 1.29 A.

H_3BTC (1 mmol), $NaOAc{\cdot}3H_2O$ (1 mmol) and two different lanthanide nitrate hydrate salts with a total molar amount of 1 mmol, $Y(NO_3)_3{\cdot}6H_2O$ (0.94 mmol) and $Ln(NO_3)_3{\cdot}6H_2O$ (0.06 mmol), where Ln = Er^{3+}, Ho^{3+}, Tm^{3+}, Yb^{3+} and Nd^{3+}, were added to a 100 ml Erlenmeyer flask. 60 ml of a mixture of DMF and distilled water (2:1, v/v) was poured to the flask which was covered with aluminium foil, mixed well and heated at 60°C for 24 h. Then, the reaction mixture was cooled to room temperature. The mixture of DMF and water was carefully decanted without pouring off the precipitate formed on the bottom. Methanol (50 mL) was then added and the solution was kept for another 24 h, while replacing MeOH once with a new amount and carefully decanting the previous portion again. The reaction product (precipitate) is separated by vacuum filtration and MeOH is used to wash the precipitate. The precipitate is then dried under vacuum for a couple of hours at 70–80°C. The data of obtained $Y_{1-x}Ln^{3+}_x(BTC)(DMF)_2(H_2O)$ synthesis products are summarised in Table 1. The theoretical stoichiometric formula of the obtained MOFs is $Y_{0.94}Ln^{3+}_{0.06}(BTC)(DMF)_2(H_2O)$, where Ln^{3+} was an exchangeable cation during each synthesis.

For the synthesis of MOFs with two active luminescent centres BTC (1 mmol), $NaOAc{\cdot}3H_2O$ (1 mmol) and three different lanthanide nitrate hydrate salts with a total molar amount of 1 mmol, $Yb(NO_3)_3{\cdot}5H_2O$ (0.20 mmol), $Y(NO_3)_3{\cdot}6H_2O$ (0.80 – x_{1-5} mmol) and $Ln(NO_3)_3{\cdot}5H_2O$ (x_{1-5} mmol, where x_{1-5} = 0.005, 0.01, 0, 02, 0.04 and 0.08 mmol), where Ln^{3+} = Er^{3+}, Ho^{3+} and Tm^{3+}, were used. The rest of the synthesis procedure was performed as described above. The results of these syntheses are presented in Table 2. The theoretical stoichiometric

Table 1. **Data of $Y_{1-x}Ln^{3+}_x(BTC)(DMF)_2(H_2O)$ syntheses**

Exchangeable cation (Ln^{3+})	Precipitate	Obtained mass, g	Yield, %	Stoichiometric MOF formula	Abbreviation in text
Er^{3+}	White powder	0.186	40.1	$Y_{0.94}Er_{0.06}(BTC)(DMF)_2(H_2O)$	YErMOF
Ho^{3+}	White powder	0.200	43.1	$Y_{0.94}Ho_{0.06}(BTC)(DMF)_2(H_2O)$	YErMOF
Tm^{3+}	White powder	0.192	41.5	$Y_{0.94}Tm_{0.06}(BTC)(DMF)_2(H_2O)$	YTmMOF
Yb^{3+}	White powder	0.181	38.8	$Y_{0.94}Yb_{0.06}(BTC)(DMF)_2(H_2O)$	YYbMOF
Nd^{3+}	White powder	0.182	39.2	$Y_{0.94}Nd_v(BTC)(DMF)_2(H_2O)$	YNdMOF

Table 2. **Data of $Y_{0.8-x}Yb_{0.2}Ln^{3+}_x(BTC)(DMF)_2(H_2O)$ syntheses**

Exchangeable cation (Ln^{3+})	Precipitate	Obtained mass, g	Yield, %	Stoichiometric MOF formula	Abbreviation in text
Er^{3+}, 0.005	White powder	0.339	39.9	$Y_{0.795}Yb_{0.20}Er_{0.005}(BTC)(DMF)_2(H_2O)$	YYbErMOF-0.5
Er^{3+}, 0.01	White powder	0.344	40.5	$Y_{0.79}Yb_{0.20}Er_{0.01}(BTC)(DMF)_2(H_2O)$	YYbErMOF-1
Er^{3+}, 0.02	White powder	0.355	41.8	$Y_{0.78}Yb_{0.20}Er_{0.02}(BTC)(DMF)_2(H_2O)$	YYbErMOF-2
Er^{3+}, 0.04	White powder	0.325	38.2	$Y_{0.76}Yb_{0.20}Er_{0.04}(BTC)(DMF)_2(H_2O)$	YYbErMOF-4
Er^{3+}, 0.08	White powder	0.333	39.0	$Y_{0.72}Yb_{0.20}Er_{0.08}(BTC)(DMF)_2(H_2O)$	YYbErMOF-8
Ho^{3+}, 0.005	White powder	0.348	41.0	$Y_{0.795}Yb_{0.20}Ho_{0.005}(BTC)(DMF)_2(H_2O)$	YYbHoMOF-0.5
Ho^{3+}, 0.01	White powder	0.337	39.7	$Y_{0.79}Yb_{0.20}Ho_{0.01}(BTC)(DMF)_2(H_2O)$	YYbHoMOF-1
Ho^{3+}, 0.02	White powder	0.354	41.7	$Y_{0.78}Yb_{0.20}Ho_{0.02}(BTC)(DMF)_2(H_2O)$	YYbHoMOF-2
Ho^{3+}, 0.04	White powder	0.349	41.0	$Y_{0.76}Yb_{0.20}Ho_{0.04}(BTC)(DMF)_2(H_2O)$	YYbHoMOF-4
Ho^{3+}, 0.08	White powder	0.361	42.3	$Y_{0.72}Yb_{0.20}Ho_{0.08}(BTC)(DMF)_2(H_2O)$	YYbHoMOF-8
Tm^{3+}, 0.005	White powder	0.364	42.9	$Y_{0.795}Yb_{0.20}Tm_{0.005}(BTC)(DMF)_2(H_2O)$	YYbTmMOF-0.5
Tm^{3+}, 0.01	White powder	0.384	45.2	$Y_{0.79}Yb_{0.20}Tm_{0.01}(BTC)(DMF)_2(H_2O)$	YYbTmMOF-1
Tm^{3+}, 0.02	White powder	0.350	41.2	$Y_{0.78}Yb_{0.20}Tm_{0.02}(BTC)(DMF)_2(H_2O)$	YYbTmMOF-2
Tm^{3+}, 0.04	White powder	0.341	40.4	$Y_{0.76}Yb_{0.20}Tm_{0.04}(BTC)(DMF)_2(H_2O)$	YYbTmMOF-4
Tm^{3+}, 0.08	White powder	0.377	44.1	$Y_{0.72}Yb_{0.20}Tm_{0.08}(BTC)(DMF)_2(H_2O)$	YYbTmMOF-8

formula of the resulting MOFs corresponds to $Y_{0.8-x}Yb_{0.2}Ln^{3+}_x(BTC)(DMF)_2(H_2O)$, where Ln^{3+} was an exchangeable cation with a variable molar ratio during each synthesis.

RESULTS AND DISCUSSION

The XRD patterns of YLnMOFs are presented in Fig. 1. The structure of synthesised YErMOF was confirmed by comparing the obtained experimental XRD with the results presented by Zhang et al. [23]. Following a successful repeated synthesis, monophasic completely new YLnMOFs, in which Er^{3+} was replaced by Ho^{3+}, Tm^{3+}, Yb^{3+} and Nd^{3+}, were synthesised (see Fig. 1). The low background noise observed in the XRD patterns confirms that the newly synthesised compounds are of high phase purity and have good crystallinity. It should be noted that regardless of the lanthanide cation being doped, the intensity and width of diffraction peaks do not change significantly. This can be explained by the fact that the structure of YMOF is doped with a small amount of Ln^{3+}. In addition, the difference of ionic radii of the lanthanides is negligible [24].

No significant background noise is also seen in the XRD patterns of YYbLnMOFs-2 (Fig. 2). This again shows that the new MOFs possess a high phase purity and good crystallinity. Also, no big differences between the XRD patterns of MOFs doped with different cations are seen. However, the amount of Yb^{3+} in the YYbLnMOFs-2 has effect on the crystallinity of synthesised compounds. Comparing the influence of Yb^{3+}, which has a high

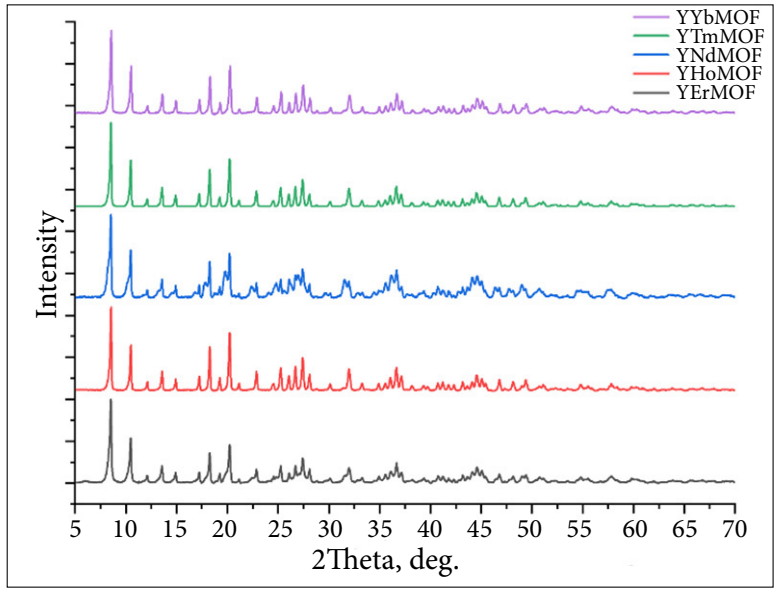

Fig. 1. XRD patterns of YLnMOFs, where Ln^{3+} = Er^{3+}, Ho^{3+}, Tm^{3+}, Yb^{3+} and Nd^{3+}. Coloured online

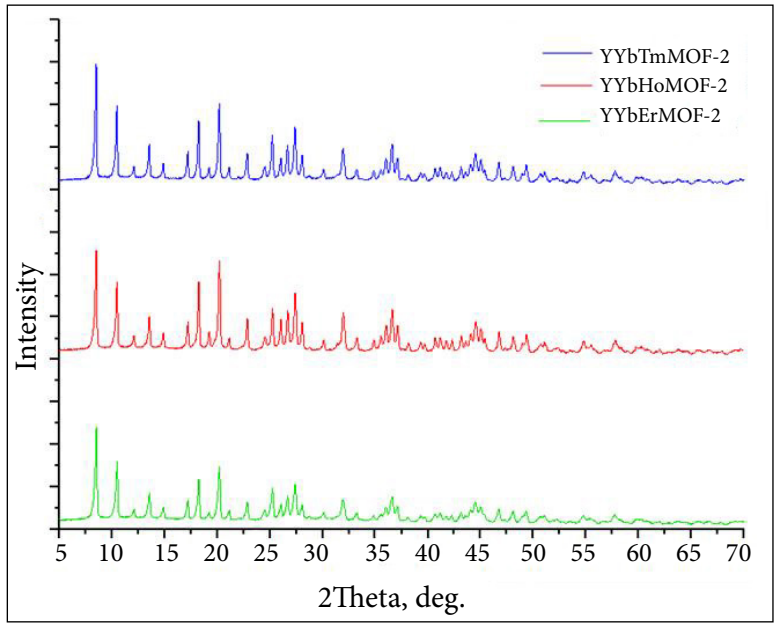

Fig. 2. XRD patterns of YYbLnMOFs-2, where Ln^{3+} = Er^{3+}, Ho^{3+} and Tm^{3+}. Coloured online

concentration in YYbLnMOF compounds up to 20%, an obvious difference is observed between the 2Θ values of 15 and 25 degrees, where the intensity of the peaks increases significantly with increasing an amount of the Ln^{3+} (Fig. 3).

The TG/DTG/DSC curves recorded for the synthesised MOFs are presented in Fig. 4. The mass losses are clearly indicated in the TG/DTG curves. As seen, with increasing temperature up to 350°C three 3 identifiable mass losses could be determined. The first mass loss, visible from 64 to 95°C, is associated with evaporation of methanol (boiling point = 64.7°C [25]) and a methanol-water azeotropic mixture. Residual MeOH in the MOF sample is possible due to changing the solvents during the purification step and the mixture of DMF and water solvents. The second mass loss can be attributed to the evaporation of DMF (boiling temp. = 153.0°C [26]), which takes place over a wider temperature range starting at ~150°C.

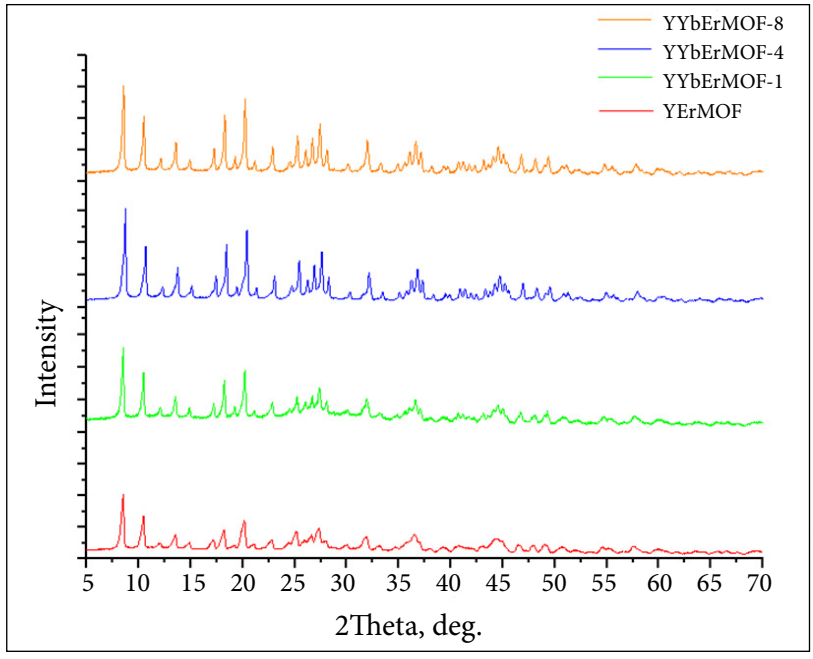

Fig. 3. XRD patterns of YYbLnMOFs with a different amount of Yb^{3+}. Coloured online

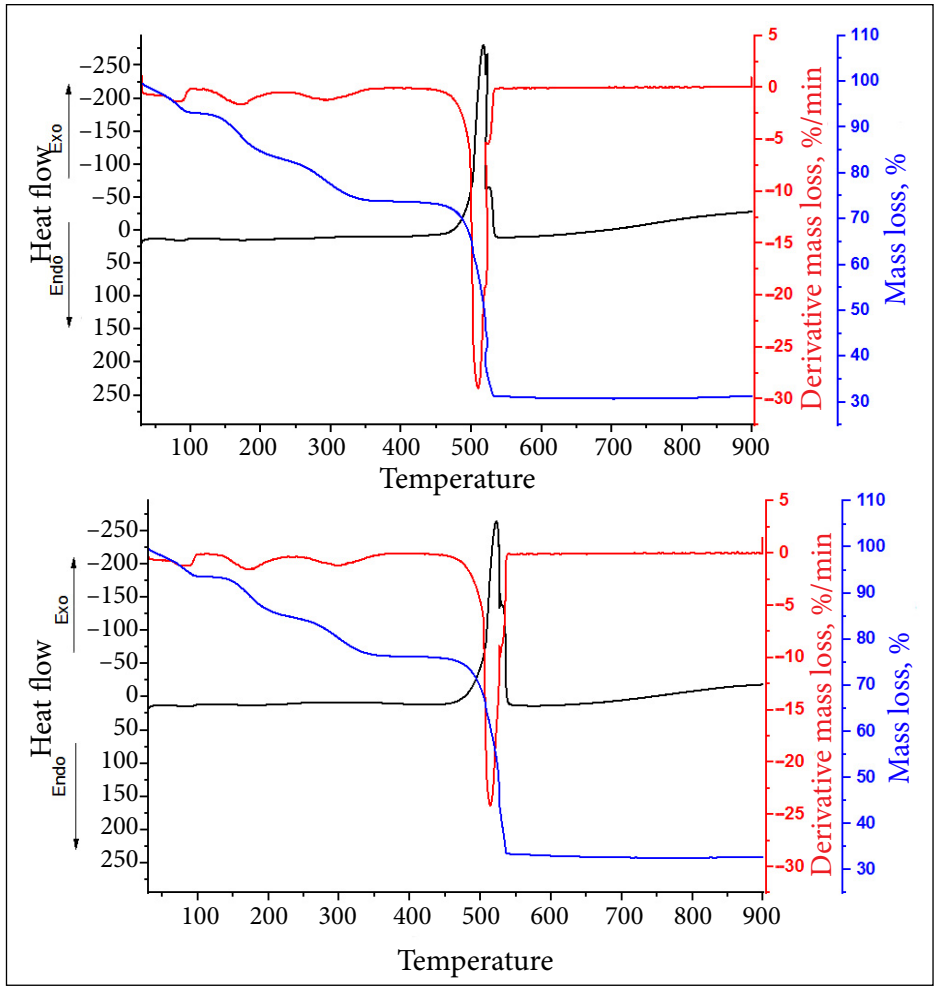

Fig. 4. TG/DTG/DSC curves of $Y_{0.94}Er_{0.06}(BTC)(DMF)_2(H_2O)$ (top) and $Y_{0.79}Yb_{0.20}Ho_{0.01}(BTC)(DMF)_2(H_2O)$ (bottom) MOFs. Coloured online

The last mass loss in the specified range up to 350°C represents degradation of the whole MOF structure (BTC melting point = 374–376°C declared by the manufacturer Alfa Aesar [27]), it occurs in a temperature range of 300–360°C. All of these processes account for about 24–25% of the weight loss. Solvent evaporation accounts for MeOH up to 6.5% and DMF up to 7.5% mass loss. In terms of heat flow, the processes are slightly endothermic (up to a maximum of 15 mW of heat absorbed), which is characteristic of evaporation and melting.

The most intensive mass loss in the TG/DTG curves is observed at 510–514°C. About 42–43% of the material is lost during this stage. The metal organic framework of benzene-1,3,5-tricarboxylic acid completely decomposes. This is demonstrated by the strongly exothermic process (heat flow value about –265 mW) – thermal decarboxylation. Further decomposition products in this temperature range are likely to correspond to Ln_2O_3 and $Ln_2(CO_3)_3$ [28, 29]. The remaining ~31–33% of the material consists of inorganic lanthanide oxides and carbonates. MOF maintains thermal stability up to ~150°C when DMF evaporation begins. According to the literature [30], a consistent drop in the mass loss curve represents MOF decomposition.

The SEM data revealed (Fig. 5) that the MOFs with two luminescent centres form rod-shaped crystalline structures with Er^{3+} and Ho^{3+}, ranging in size about 1.0–2.0 μm. However, the MOF with Tm^{3+} (see Fig. 5c) is composed of rectangular crystals about 1.0 μm in size.

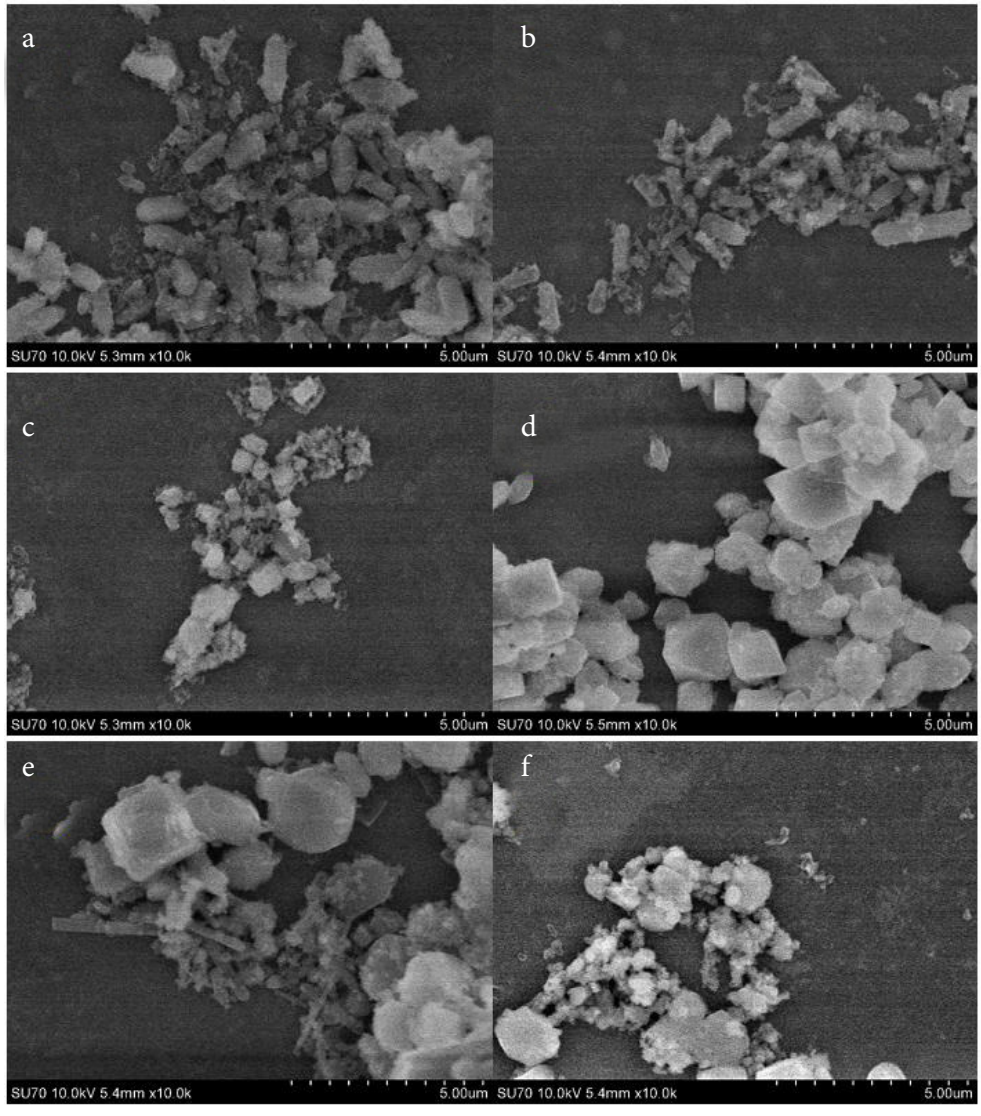

Fig. 5. SEM micrographs of YYbErMOF-4 (a), YYbHoMOF-4 (b), YYbTmMOF-4 (c), YErMOF (d), YHoMOF (e) and YTmMOF (f). Magnification 10 000

In the MOF compounds with one luminescent centre ($Y_{1-x}Ln^{3+}_x(BTC)(DMF)_2(H_2O)$) the shape of the crystals varies from cubic (with Er^{3+}) to irregular rectangles (with Ho^{3+}), but their size remains unchanged in a range of 1.0–2.0 μm. The MOF crystals with Tm^{3+} have an irregular microstructure, having mostly a rectangular shape and a size about 1.0 μm. The surface microstructure of synthesised MOFs particles with Nd^{3+} and Yb^{3+} is very similar to the microstructure of MOF crystals with Tm^{3+}.

Thus, the microstructure of synthesised $Y_{1-x}Ln^{3+}_x(BTC)(DMF)_2(H_2O)$ and $Y_{0.8-x}Yb_{0.2}Ln^{3+}_x(BTC)(DMF)_2(H_2O)$ MOFs is slightly dependent on the nature of a lanthanide element.

Based on the literature review, synthesised MOFs would be consistent with the GSA/ETU conversion mechanism. Emission spectra of 6% (optically inactive Y^{3+} ions filling the rest of the crystalline matrix) of Er^{3+}, Ho^{3+}, Tm^{3+}, Nd^{3+} and Yb^{3+} MOFs compounds were recorded after excitation with 980 nm laser radiation. Of the five different lanthanide cations, only Er^{3+} containing $Y_{0.94}Er_{0.06}(BTC)(DMF)_2(H_2O)$ MOF exhibited upconversion properties (Fig. 6).

In the emission spectrum of $Y_{0.94}Er_{0.06}(BTC)(DMF)_2(H_2O)$ three distinct peaks of different types (triplet, doublet and triplet forms, respectively) can be identified. The first two peaks correspond to a green emission (at 523 and 547 nm, the latter being the most intense), and the third peak represents a red emission (669 nm). Based on the literature data [3, 31], electron transitions $^2H_{11/2} \rightarrow {}^4I_{15/2}$, $^4S_{3/2} \rightarrow {}^4I_{15/2}$ and $^4F_{9/2} \rightarrow {}^4I_{15/2}$, respectively, were observed. All emission peaks are quite narrow and correspond to the Er^{3+} specific emission. A very low intensity peak at 412 nm can also be observed in the emission spectrum. According to the literature [32], this may correspond to a $^2H_{9/2}$ transition.

Another peak of even lower intensity in this spectrum is at 701 nm (red emission). However, the intensity of this peak is very low and is not attributed to the characteristic emission of Er^{3+} ions.

Emission spectra of Yb^{3+}, Ho^{3+}, Tm^{3+} and Nd^{3+} metal organic frameworks yielded no informative data. It can be stated that the latter ions do not have favourable energy levels for successful upconversion under the single fluorescent centre GSA/ETU conversion mechanism. It can also be stated by analogy that the BTC anion is not suitable for upconversion. This carboxylic acid does not have a sufficient conjugated π system in the benzene ring along with a carboxylic acid moiety, which would allow BTC to act as a sensitizer in upconversion initiation by the TTA-UC mechanism.

Following these results, it was decided to try to synthesise MOF compounds with two fluorescent centre that could correspond to a GSA/ETU type conversion mechanism. In this case, the most effective lanthanide pairs discussed in the literature from the activator-sensitizer were selected: Er^{3+}–Yb^{3+}, Ho^{3+}–Yb^{3+} and Tm^{3+}–Yb^{3+} (Y^{3+} ions were filling the rest crystalline matrix). The amount of

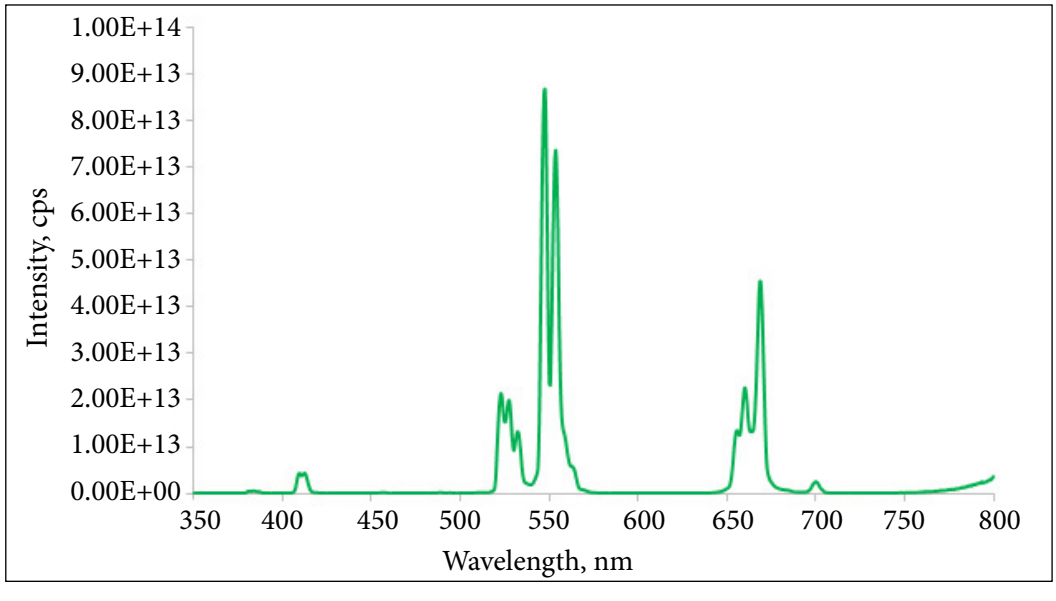

Fig. 6. Emission spectrum of $Y_{0.94}Er_{0.06}(BTC)(DMF)_2(H_2O)$ MOF. Coloured online

Yb^{3+} ions was maintained in two fluorescent centre MOFs at 0.2 mmol, and acted as a sensitizer in these compounds. To estimate which concentration of activators gives the highest intensity in the emission spectra, their concentrations were doubled from 0.005 to 0.08 mmol each time. A total of five different concentrations of MOF compounds for each ion pair of two luminescent centres were investigated. After the excitation with 980 nm radiation, emission spectra were measured. However, an unusual phenomenon was observed. During the measurement by focusing the laser beam on the powder in the cuvette, MOFs of all three different ion pairs, regardless of the minimum or maximum (0.1–1 W) laser power intensity, burned to charring. In this way, it was not possible to determine the same laser power intensity and focus for different samples. Therefore, a comparison of the intensities of different activator concentrations could not be objective because of the different measurement conditions for each compound in the series.

No justification could be found in the literature for this charring phenomenon. The essential condition that varied between measurements at one (up to 6% concentration) and two luminescence centres (20% Yb^{3+} and 0.5–8% replaceable activator Ln^{3+}) was an increase in the Yb^{3+} ion concentration of more than three times (compared to not charred $Y_{0.94}Yb_{0.06}(BTC)(DMF)_2(H_2O)$). Yb^{3+} ions effectively absorb 980 nm laser radiation. It can be hypothesised that, due to unknown processes, the concentration of this ion was too high in these MOF compounds. Tm^{3+}–Yb^{3+} MOFs did not exhibit upconversion properties and did not emit a visible spectrum. However, the upconversion phenomenon was recorded using Er^{3+} and Ho^{3+} as an activator. The emission spectrum of $Y_{0.76}Yb_{0.20}Er_{0.04}(BTC)(DMF)_2(H_2O)$ is shown in Fig. 7.

The $Y_{0.76}Yb_{0.20}Er_{0.04}(BTC)(DMF)_2(H_2O)$ emission spectrum displayed doublet (at 627 and 639 nm) and triplet (at 654, 668 and 682 nm) peaks. The most intensive triplet peak coincided with the most intensive peak of the $Y_{0.94}Er_{0.06}(BTC)(DMF)_2(H_2O)$ triplet. Thus, in the $Y_{0.76}Yb_{0.20}Er_{0.04}(BTC)(DMF)_2(H_2O)$ case, this emission spectrum peak corresponds to the characteristic $^4F_{9/2} \rightarrow {}^4I_{15/2}$ electron transition. An intensive doublet in the emission spectrum is not entirely characteristic of the Er^{3+} ion. According to the Dieke diagram [33], an erbium trivalent ion does not have an energetic level similar to that of $^4F_{9/2}$, which could be attributed to the intensive peak in the spectrum doublet (see Fig. 7). Therefore, the relaxation jump of this peak may not occur to the unexcited state of $^4I_{15/2}$ at the lowest energy level. This can be explained by following

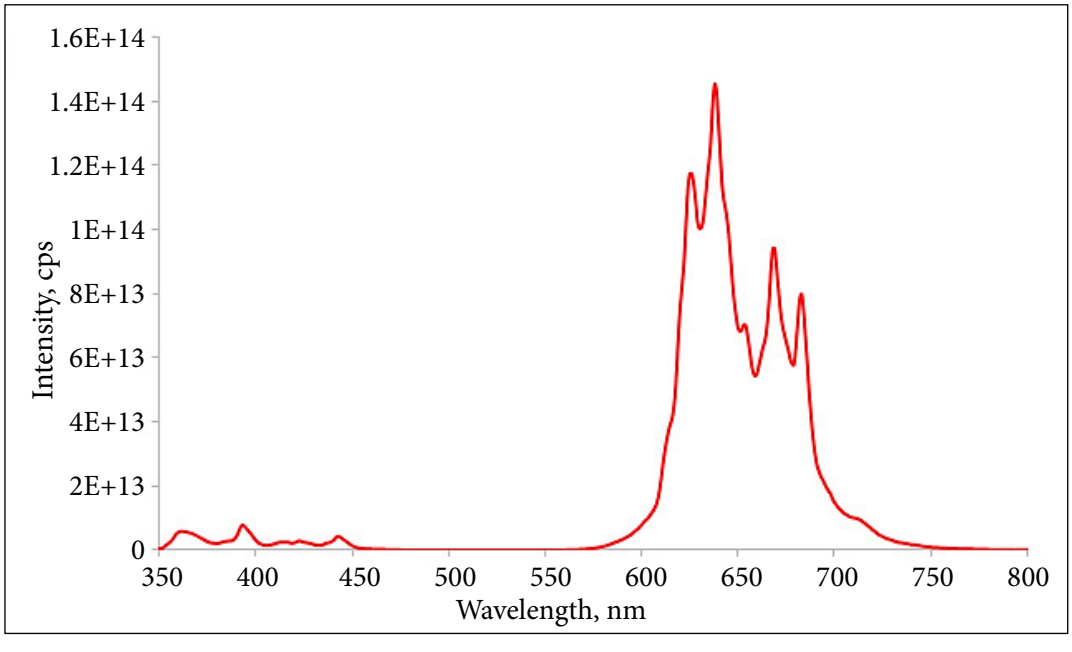

Fig. 7. Emission spectrum of $Y_{0.76}Yb_{0.20}Er_{0.04}(BTC)(DMF)_2(H_2O)$. Coloured online

the Dieke diagram. The closest and higher energy than the $^4F_{9/2}$ excited level is only the $^4S_{3/2}$ level. However, the relaxation transition from this level to the unexcited state is a typical green emission. The emission spectrum of $Y_{0.76}Yb_{0.20}Er_{0.04}(BTC)(DMF)_2(H_2O)$ also did not display a green emission in comparison to the emission spectrum of $Y_{0.94}Er_{0.06}(BTC)(DMF)_2(H_2O)$.

The emission spectrum of $Y_{0.79}Yb_{0.20}Ho_{0.01}(BTC)(DMF)_2(H_2O)$ (Fig. 8) revealed a sharp peak at 418 nm (purple). The literature review did not provide such a characteristic Ho^{3+} emission.

According to the Dieke diagram, this transition would be difficult to attribute to a specific transition towards an unexcited level, because in the 26–30·10^3 cm^{-1} energy range a trivalent Ho^{3+} ion has many similar energy levels. The remaining peaks of $Y_{0.79}Yb_{0.20}$ $Ho_{0.01}(BTC)(DMF)_2(H_2O)$ emission are located at 594 and 615 nm (orange), as well as at the 640 and 652 nm peak (red). The latter corresponds to a characteristic (mentioned in the literature review at 647 nm) electron transition $^5I_4 \rightarrow {}^5I_8$. According to the Dieke diagram [33], the 640 nm peak corresponds to the transition from the excited state of $^5F_5$ to $^5I_8$.

In conclusion of this study, XRD analysis results displayed the monophasic $Y_{1-x}Ln^{3+}_x(BTC)(DMF)_2(H_2O)$ MOFs of one luminescence centre (Ln^{3+} = Yb^{3+}, Ho^{3+}, Tm^{3+} and Nd^{3+}) and $Y_{0.8-x}Yb_{0.2}Ln^{3+}_x(BTC)(DMF)_2(H_2O)$ MOFs of two luminescence centres (Ln^{3+} = Er^{3+}, Ho^{3+} and Tm^{3+}) were successfully synthesised using a simple crystallisation method. The obtained MOFs were found to be thermally stable up to 150°C. The upconversion properties of the synthesised MOFs were investigated. It has been found that in the case of one luminescent centre, Er^{3+} can be used as an activator for successful upconversion, and in the case of two luminescent centers, Yb^{3+}–Er^{3+} and Yb^{3+}–Ho^{3+} can be used as sensitizer-activator pairs. It was concluded that Yb^{3+}, Ho^{3+}, Tm^{3+} and Nd^{3+} cations are unsuitable as activators for the upconversion for one luminescent centre, and the Yb^{3+}–Tm^{3+} pair is unsuitable for two luminescent centres of MOF type. It has been also shown that the benzene-1,3,5-tricarboxylic acid (BTC) anion cannot act as a upconversion sensitizer for the TTA-UC mechanism.

ACKNOWLEDGEMENTS

This work was supported by a Research Grant NEGEMAT (No. S-MIP-19-59) from the Research Council of Lithuania.

Received 15 March 2021
Accepted 22 April 2021

References

1. F. Auzel, *Chem. Rev.*, **104**(**1**), 139 (2004).
2. F. E. Auzel, *IEEE*, **61**(**6**), 758 (1973).
3. A. Nadort, J. Zhao, E. M. Goldys, *Nanoscale*, **8**(**27**), 13099 (2016).

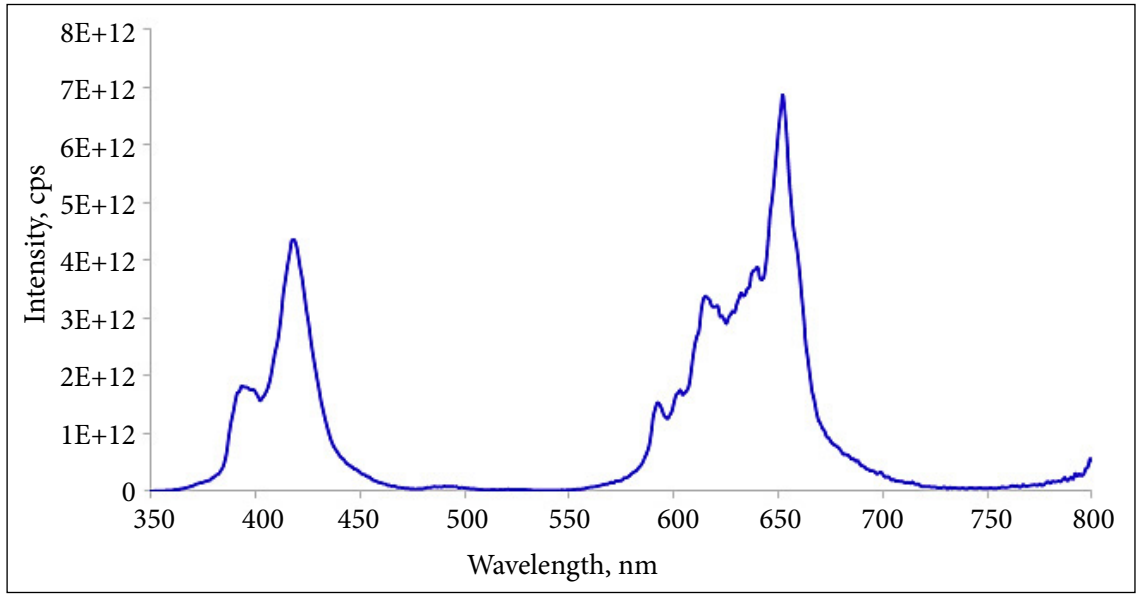

Fig. 8. Emission spectrum of $Y_{0.79}Yb_{0.20}$ $Ho_{0.01}(BTC)(DMF)_2(H_2O)$. Coloured online

4. Y. O. M. Rosi, J. Eckert, M. Eddaoudi, et al., *Science*, **300**(**5622**), 1127 (2007).
5. D. W. Lim, H. Kitagawa, *Chem. Rev*., **120,** 8416 (2020).
6. S. Horike, S. S. Nagarkar, T. Ogawa, S. Kitagawa, *Angew. Chem. Int. Ed.*, **59**(**17**), 6652 (2020).
7. X. Zhang, B. Wang, A. Alsalme, S. Xiang, Z. Zhang, B. Chen, *Coord. Chem. Rev.*, **423**, 213507 (2020).
8. D. M. Kabtamu, Y. N. Wu, F. T. Li, *J. Hazard. Mater*., **397**(**1227**) (2020).
9. B. Li, H.-M. Wen, W. Zhou, B. Chen, *J. Phys. Chem. Lett.*, **5**(**20**), 3468 (2014).
10. C. A. Grande, R. Blom, V. Middelkoop, et al., *Chem. Eng. J*., **402**, 126 (2020).
11. J. Li, J. Sculley, H. Zhou, *Chem. Rev.*, **112**(**2**), 869 (2012).
12. D. Ursueguia, E. Diaz, A. Vega, S. Ordonez, *Separ. Purif. Technol*., **251** (2020).
13. M. Pintado-Sierra, A. M. Rasero-Almansa, A. Corma, M. Iglesias, F. Sánchez, *J. Catal.*, **299**, 137 (2013).
14. S. Rostamnia, H. Alamgholiloo, X. Liu, *J. Colloid Interface Sci.*, **469**, 310 (2016).
15. Y. Zhang, X. Yang, H.-C. Zhou, *Polyhedron*, **154**, 189 (2018).
16. A. Laurikėnas, F. Yalçin, R. Žilinskas, et al., *Chemija*, **30**, 89 (2019).
17. E. S. Degtyareva, K. S. Erokhin, V. P. Ananikov, *Catal. Commun*., **146** (2020).
18. K. Müller-Buschbaum, *Ref. Mod. Chem. Molec. Sci. Chem. Eng.*, **1** (2015).
19. P. Wang, R. Fan, Y. Yang, X. Liu, W. Cao, B. Yang, *J. Solid State Chem.*, **196**, 441 (2012).
20. A. Laurikenas, A. Katelnikovas, R. Skaudzius, A. Kareiva, *Opt. Mat.*, **83**, 363 (2018).
21. M. Fumanal, C. Corminboeuf, B. Smit, I. Tavernelli, *Phys. Chem. Chem. Phys*., **22**, 19512 (2020).
22. P. Silva, S. M. F. Vilela, J. P. C. Tomé, F. A. Almeida Paz, *Chem. Soc. Rev.*, **44**(**19**), 6774 (2015).
23. X. Zhang, B. Li, H. Ma, L. Zhang, H. Zhao, *ACS Appl. Mater. Interfaces*, **8**(**27**), 17389 (2016).
24. R. D. Shannon, *Acta Cryst*., **32**(**5**), 751 (1976).
25. J. Wang, X. Li, H. Meng, C. Li, Z. Wang, *J. Chem. Thermodyn*., **41**(**2**), 167 (2009).
26. E. W. Jones, P. J. Holliman, A. Connell, M. L. Davies, *Chem. Commun*., **52**, 4301 (2016).
27. D. J. Duchamp, R. E. Marsh, *Acta Cryst. B*, **25**, 5 (1969).
28. S.-P. Chen, Y.-X. Ren, W.-T. Wanga, S.-L. Gao, *Dalton Trans*., **39**, 1552 (2010).
29. A. Kareiva, M. Karppinen, L. Niinistö, *J. Mater. Chem.*, **4**, 1267 (1994).
30. X Guo, G. Zhu, Z. Li, Y. Chen, X. Li, S. Qiu, *Inorg. Chem*., **45**(**10**), 4065 (2006).
31. J. Zhou, Q. Liu, W. Feng, Y. Sun, F. Li, *Chem. Rev*., **115(1)**, 395 (2014).
32. W. Ma et al., *J. Opt. Soc. Am*., **6**(**2**), 409 (2016).
33. G. H. Dieke, H. M. Crosswhite, *Appl. Opt*., **2**(**7**), 675 (1963).

Andrius Laurikėnas, Aivaras Kareiva

APKONVERSIJOS TYRIMAS $Y_{1-X}LN^{3+}_{X}(BTC)(DMF)_2(H_2O)$ IR $Y_{0.8-X}YB_{0.2}LN^{3+}_{X}(BTC)(DMF)_2(H_2O)$ METALOORGANINĖSE STRUKTŪROSE

S a n t r a u k a

Tyrime buvo sintetinamos ir tiriamos $Y_{1-x}Ln^{3+}_{x}(BTC)(DMF)_2(H_2O)$ ir $Y_{0.8-x}Yb_{0.2}Ln^{3+}_{x}(BTC)(DMF)_2(H_2O)$ metaloorganinės struktūros (MOF), kurių sudėtyje yra Er^{3+}, Ho^{3+}, Tm^{3+}, Yb^{3+}, Nd^{3+} jonų. Buvo analizuojami gautųjų junginių apkonversijos parametrai. Šiuo tikslu organinės dalies pirmtakas buvo pasirinktas benzen-1,3,5-trikarboksirūgštis (BTC) kaip vienas paprasčiausių ir dažnai literatūroje cituojamų karboksirūgšties ligandų MOF sintezėse. Charakterizuojant gautųjų MOF apkonversines savybes buvo nustatyta, kad esant vienam liuminescencijos centrui Er^{3+} gali būti panaudojamas kaip aktyvatorius, o Yb^{3+}, Ho^{3+}, Tm^{3+} ir Nd^{3+} jonai neturi tinkamos elektroninės konfigūracijos apkonversijai vykti pagal nesužadintos būsenos absorbcijos–sužadintos būsenos absorbcijos (GSA/ESA) mechanizmą. Taip pat BTC negali inicijuoti tripletinės–tripletinės anihiliacijos apkonversijos (TTA-UC) kaip šio mechanizmo sensibilizatorius. Esant dviem liuminescenciniams centrams yra tinkamos Yb^{3+}-Er^{3+} ir Yb^{3+}-Ho^{3+} jonų poros kaip sensibilizatoriaus–aktyvatoriaus pora pagal GSA/energijos perdavimo apkonversijos (GSA/ETU) mechanizmą. Yb^{3+}-Tm^{3+} pora, priešingai nei rodo pavyzdžiai literatūroje, nepasižymėjo apkonversinėmis savybėmis susintetintose metaloorganinėse struktūrose.